Todorov, Oleg; Alanne, Kari; Virtanen, Markku; Kosonen, Risto

A method and analysis of aquifer thermal energy storage (ATES) system for district heating and cooling

Published in:
Sustainable Cities and Society

DOI:
10.1016/j.scs.2019.101977

Published: 01/02/2020

Document Version
Publisher's PDF, also known as Version of record

Sustainable Cities and Society 53 (2020) 101977

Contents lists available at ScienceDirect

Sustainable Cities and Society

journal homepage: www.elsevier.com/locate/scs

A method and analysis of aquifer thermal energy storage (ATES) system for district heating and cooling: A case study in Finland

Oleg Todorov[a,*], Kari Alanne[a], Markku Virtanen[a], Risto Kosonen[a,b]

[a] Department of Mechanical Engineering, School of Engineering, Aalto University, Finland
[b] Nanjing Tech University, College of Urban Construction, PR China

ARTICLE INFO

Keywords:
Aquifer thermal energy storagege
Groundwater heat pump
District heating and cooling
Holistic integration
Groundwater modeling
MODFLOW

ABSTRACT

Aquifer thermal energy storage (ATES) systems with groundwater heat pumps (GWHP) provide a promising and effective technology to match the renewable energy supply and demand between seasons. This paper analyses the integration of an ATES and GWHP system in both district heating (DH) and district cooling (DC) networks in terms of system's efficiency, techno-economic feasibility and impact on the surrounding groundwater areas. To that end, a novel method of holistic integration of groundwater modeling is proposed and demonstrated for retrieving and analyzing data from a variety of open Finnish public data sources. A case study is presented, where the ATES integration is examined within an existing district heating network in Southern Finland. It is concluded that combining heating and cooling, with seasonally reversible ATES operation and balanced pumping volumes during summer and winter periods, had low impact on the aquifer area and is economically feasible. Finally, the study concludes that even with limited data, obtained from open public data sources, it is possible to assess the ATES integration with an acceptable accuracy.

1. Introduction

Buildings in Europe account for 41 % of the final energy consumption, followed by transport (32 %), and industry (25 %) (EU, 2013). In line with the Paris Agreement, carbon neutrality should be obtained by 2050 (UN, 2015). Hence, the integration of renewable energy technologies in heating and cooling of buildings and communities is a necessity. Since the variations of the availability of renewable energy between heating and cooling seasons are significant, a seasonal storage is needed to maximize the usage of renewable energy. One of the most promising technological options is Aquifer Thermal Energy Storage (ATES) due to its relative affordability and ability to enable large storage capacities (Pellegrini et al., 2019). Furthermore, by utilizing the available subsurface space in cities, ATES systems can potentially provide sustainable heating and cooling energy for different building typologies, thus the ATES integration in a district/urban level can be more efficient and resilient compared to a conventional separate heating and cooling generation (Hooimeijer & Maring, 2018). ATES heat storage is based on mature technologies, with groundwater heat pump (GWHP) as a core of an ATES system. The research interest in shallow (< 300 m of depth) geothermal energy systems is more recent, dating back to the 1970's (Sanner, Systems, Systems, & Pumps, 2001).

The potential of ATES technology to be integrated as a sub-system of sustainable space heating and cooling in tandem with the recovery of heat in the subsurface has been acknowledged worldwide. According to Fleuchaus, Godschalk, Stober, and Blum (2018), there were around 3000 ATES systems in the world in 2017, mostly concentrated in Europe. The Nordic countries and particularly the Netherlands (2500), Sweden (220) and Denmark (55) are the frontrunners of ATES application. According to Schmidt, Pauschinger, Sørensen, Snijders, and Thornton (2018), from these 3000 ATES projects, there are 100 large-scale systems integrated in district heating and cooling (DH/DC) networks. The research of Paiho et al. (2018) revealed that large-scale heat pumps can increase the flexibility of the district heating system, especially when utilizing heat pumps for first-stage preheating before the CHP-plant finally adjusts the supply temperature. In the same study are given several examples for heat pump utilization in DH/DC networks in Finland – the Kakola plant in Turku utilizing heat from waste water and

Abbreviations: ATES, aquifer thermal energy storage; COP, coefficient of performance; DC, district cooling; DH, district heating; FDM, finite difference method; GIS, Geographic Information System; GRD, surfer grid file extension; GTK, Geological Survey of Finland; GWHP, ground water heat pump; LGR, local grid refinement; NLSF, National Land Survey of Finland; RMSE, root mean squared error; SYKE, Finnish Environmental Institute; TIFF, Tagged Image File Format; USGS, United States Geological Survey

* Corresponding author at: Department of Mechanical Engineering, School of Engineering, Aalto University, Sähkömiehentie 4, 02150 Espoo, Finland.
E-mail address: oleg.todorovradoslavov@aalto.fi (O. Todorov).

https://doi.org/10.1016/j.scs.2019.101977
Received 2 July 2019; Received in revised form 1 October 2019; Accepted 18 November 2019
Available online 20 November 2019

Nomenclature

α	Longitudinal dispersivity [m]
AF	Annuity factor
a	Cell size of square discretization grid [m]
b	Aquifer thickness [m]
c_m	Aquifer material heat capacity [J/kg K]
c_s	Solid material heat capacity [J/kg K]
c_w	Water heat capacity [J/kg K]
D_m	Molecular diffusion coefficient [m^3/kg]
Φ	Energy demand (heating/cooling) [W]
h	Hydraulic head [m]
i	Hydraulic gradient [m/m]
K	Hydraulic conductivity [m/s]
K_d	Distribution coefficient [m^2/s]
λ_m	Aquifer material thermal conductivity [W/mK]
λ_s	Solid material thermal conductivity [W/mK]
λ_w	Water thermal conductivity [W/mK]
n	Aquifer porosity [%]
P	Power demand (pumping) [W]
q	Flux, specific discharge [m/s]
Q	Volume flow rate of source/sink [m^3/s]
r	Interest rate
R	Aquifer recharge [m/s]
ρ_b	Dry bulk density [kg/ m^3]
ρ_m	Aquifer material density [kg/ m^3]
ρ_s	Solid material density [kg/ m^3]
ρ_w	Water density [kg/ m^3]
s	Drawdown [m]
S	Storativity
S_s	Specific storage [1/m]
S_y	Specific yield [%]
$S_{VC,aq}$	Aquifer volumetric heat capacity [J/m^3K]
$S_{VC,wat}$	Water volumetric heat capacity [J/m^3K]
T	Transmissivity [m^2/s]

the Katri Vala plant in Helsinki producing DH and DC in a single process.

Bloemendal, Olsthoorn, and van de Ven (2015) developed a method for identifying the available world ATES potential combining climatic and hydro-geological data, as well as elaborated a world map for ATES suitability. The study concluded that some 50 % of world urban areas have medium potential for ATES (remaining stable among the present century), while 15 % have high potential - a figure which will decrease to 5 % in the second half of 21st century due to climate change. Lu, Tian, and He (2019) presented similar approach for evaluating world ATES potential based on socio-economic, geo-hydrological, climatic and groundwater factors, as well as concluded that ATES potential is very good, good and moderate in 7 %, 20 % and 34 % of the zones respectively. Arola and Korkka-Niemi (2014) have concluded that especially for high density urban areas, the undisturbed groundwater temperature could be even 3 – 4 °C higher than the average air temperature due to the heat island effect. Bayer, Attard, Blum, and Menberg (2019) coined the concept of subsurface urban heat islands (SUHI) and concluded that large-scale urban subsurface temperature could be 2 – 6 °C higher than in the countryside. The research of Bonafoni, Baldinelli, and Verducci (2017) suggested the utilization of satellite remote sensing analysis of albedo and surface temperature changes in order to control the increase of SUHI effect in cities. Consequently, cities, at least in Nordic conditions where heat extraction from ground is dominant, are the perfect candidates for ATES development and integration. Multiple research works so far have been focused on ATES planning/monitoring in high density urban areas in terms of optimization of available subsurface space, flow/thermal interference and ATES overall efficiency (Bakr, van Oostrom, & Sommer, 2013; Bloemendal, Olsthoorn, & Boons, 2014; Bloemendal, Jaxa-Rozen, & Olsthoorn, 2018; Bozkaya, Li, Labeodan, Kramer, & Zeiler, 2017; Caljé, 2010; Fleuchaus, Schüppler, Godschalk, Bakema, & Blum, 2020; Hoving et al., 2014; Sommer, Valstar, Leusbrock, Grotenhuis, & Rijnaarts, 2015).

It has been concluded that realizing a sustainable ATES system requires long-term balancing of charging and discharging the storage. Additionally, the system's performance can be optimized by storing extra heat or cooling capacity from other (sustainable) sources e.g. by using solar thermal harvesting (Ghaebi, Bahadori, & Saidi, 2014; Kastner et al., 2017; Paksoy, Andersson, Abaci, Evliya, & Turgut, 2000). Optimization can be achieved also by controlling the energy exchange between warm or cold wells in individual ATES systems taking into account its impacts on the neighboring ATES systems or by modifying the energy demand itself (demand side management). Here, groundwater heat pumps (GWHP) take advantage of stable subsurface temperatures and the ability of groundwater areas to store the excess energy in order to use it when necessary (seasonal shifting of energy demand). Taking also into account that groundwater temperature is annually stable and, in Northern climate, several degrees above the average air temperature, heating mode operation of GWHP is much more efficient compared to conventional air-to-air heat pumps or fossil fuel boilers.

Lund and Boyd (2016) revealed that geothermal energy penetration in Finland is high. However, it is still mostly driven by domestic and small-scale installations and practically inexistent in a large-scale/district level. Surprisingly, despite the availability of important aquifer areas and highly developed DH networks, Finland has still not implemented ATES systems in a large scale. Moreover, the availability of numerous groundwater resources in Finland is an important additional advantage for GWHP introduction and deployment, taking into account the variety of ATES projects implemented during the last decades in other Nordic countries like Sweden. For the above reasons, Finland has been chosen as the target country of the present study.

ATES operation results in a combined hydrological, thermal, chemical and microbiological impact on the affected groundwater areas and should be carefully evaluated (Bonte, Stuyfzand, Hulsmann, & van Beelen, 2011). The legislation of shallow geothermal installations (depth less than 400 m) is diverse among countries (Haehnlein, Bayer, & Blum, 2010). Regulations for installations of wells concern the use of hazardous materials and proper backfilling of the drilling hole to avoid hydraulic short circuiting between aquifers. Other legislation concerns protection of groundwater areas for drinking water supply. Some countries adopt limits for minimum and maximum storage temperatures, like Austria (5–20 °C), Denmark (2–25 °C) and the Netherlands (5–25 °C) - while others adopt a maximum change in groundwater temperature, for example Switzerland (3 °C) and France (11 °C). In Finnish legislation, there is no explicit reference to groundwater use for energy generation and storage, the only generally related laws are the Water Act (1961) and the Environmental Protection Act (2000).

Arola and Korkka-Niemi (2014) presented a theoretical study for ATES utilization in Finnish conditions, combining simulated energy demands for different building types with groundwater modeling, as well as performing separate simulations for heating/cooling loads with assumed constant heat pump COP, where finally a long-term environmental impact was assessed for each case. In Finland, there are publicly available data sources regarding the hydrological resources (Finnish Environmental Institute), geological conditions (Geological Survey of Finland) and geographical data (National Land Survey of Finland). The present work introduces a novel method for retrieving data from the aforementioned Finnish public sources and modeling the ATES system

using combined heating/cooling loads and variable COP-model for ATES integration in DH/DC networks. The present paper highlights also the importance of some calculated ATES parameters (thermal radius, heat recovery efficiency), which can be useful during pre-feasibility evaluation or in combination with more sophisticated modeling tools.

The novelty of this paper is to investigate holistically the ATES application for heating and cooling, and although using limited and uncertain data, be able to prepare a sufficiently accurate feasibility study from three different perspectives – technical rationale, economic feasibility and environmental impact. Furthermore, a simplified but holistic groundwater and techno-economic modeling approach of the energy system is introduced and developed. The present research will contribute to develop a valuable knowledge on ATES systems analysis, modeling and implementation. This work can potentially benefit engineers, energy companies and final users as well as organizations and agencies responsible for environmental legislation and energy efficiency.

2. Materials and methods

The modeling scheme of an ATES system is developed through the following general steps, namely - i) pre-processing of input data, ii) data processing using different tools & methods, and iii) post-processing with results presentation and analysis (Fig. 1). In order to adequately model an ATES system, it is fundamental to develop and calibrate a specific groundwater model. Basically, both ATES and groundwater models should be connected and linked together by using different tools for data interaction. Finite difference method-based groundwater models (MODFLOW, Harbaugh, 2005) and solute/heat transport (MT3DMS, Zheng & Wang, 1999) are adopted and developed in the present work. Models are calibrated against statistical data (observation wells) of the studied groundwater areas. In Sections 2.2–2.4, the development of the modeling methodology is explained with details and demonstrated referring to the information and data collected from the Finnish case study (introduced in Section 2.1).

2.1. Input data for ATES design

2.1.1. Characterization of the district heating network

In the design process, the first step is to characterize the target district heating network, which is in this case study located in the village of Pukkila, a Finnish municipality located in the Uusimaa region in the southern part of Finland, and its heat is mainly produced by wooden chips in a 1.5 MW nominal boiler. In addition to the base load chips boiler, the heating plant has two peak load oil boilers (2 MW), which have been used sporadically. The annual district heat generation in Pukkila was 4407 MW h in 2017 and a daily- based power demand is presented in Fig. 2 (Hynynen, 2018a, b). The efficiency of the base load boiler (chips) is estimated to be about 80 % (Hynynen, 2018a).

2.1.2. Characterization of groundwater areas

In the second step, available data is retrieved from open Finnish public sources in order to characterize the groundwater areas. Here, data from Finnish Environment Institute (Suomen Ympäristökeskus, SYKE) website is used (https://www.syke.fi/en), and particularly Hertta 5.7 application regarding groundwater areas, as well as monitoring stations and observation wells. Pukkila's groundwater area is composed of three different aquifer zones, of which two (Vanhalanmäki-161602 and Pukkilan kk-161601) are close to Pukkila village and its district heating plant. Porvoonjoki River is a natural border of the south-eastern part of the village and separates area 161,601 in two parts, being also a specified head boundary for the studied area (see Fig. 3).

There is available information for 5 observation wells in area 161,602 (# 105, 205, 305, 405 and 505) and 5 observation wells in area 161,601 (# 605, 705, 805, 905 and 1005). The water level variation of each well has been recorded during the last 10 years and the average values were used for the steady state model calibration. Observations have revealed an average aquifer temperature of 6.5 − 7 °C (Arola, 2018).

2.1.3. Geographical data (elevation model)

The third step of the design process is to assess and model appropriately the groundwater flow as well as to establish correctly the boundary conditions, starting with reliable terrain model. The open data of the National Land Survey of Finland (https://tiedostopalvelu.maanmittauslaitos.fi/tp/kartta?lang=en), particularly its "10 m elevation model" is used for this purpose. The elevation model was downloaded as Geo-TIFF raster file in two separate cadastral sheets, L4111 and L4112, converted to Surfer Grid file (GRD) using QGIS (QGIS, 2019). The extracted area of roughly 5.2 km in length and 1.3 km in width contains a dynamic terrain with elevations between roughly 35 and 95 m a.s.l., as seen in Fig. 4. The Porvoonjoki River and its effluents Virenoja and Kuutinoja determine the hydrogeological contours and will play a key role as natural boundaries of the groundwater model.

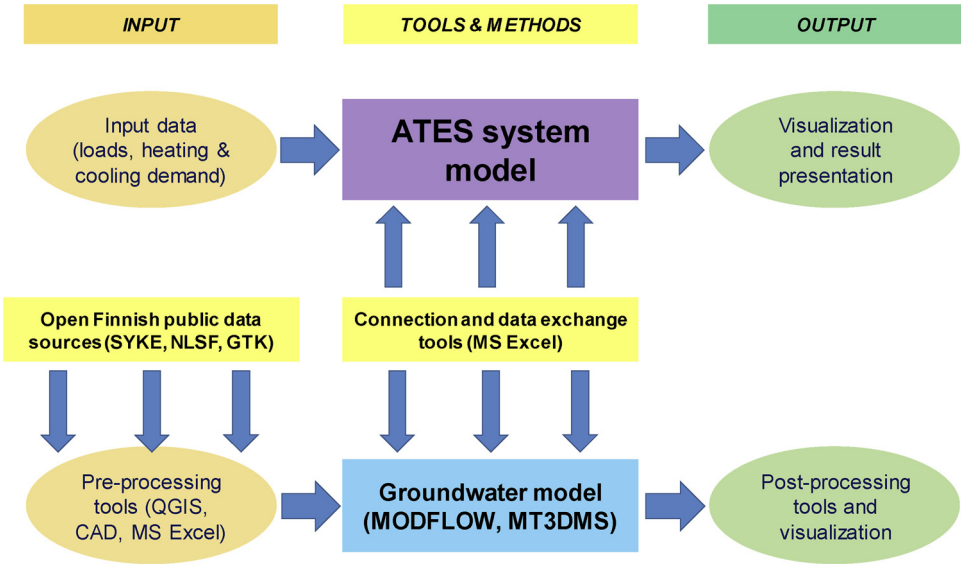

Fig. 1. Modeling scheme of ATES system.

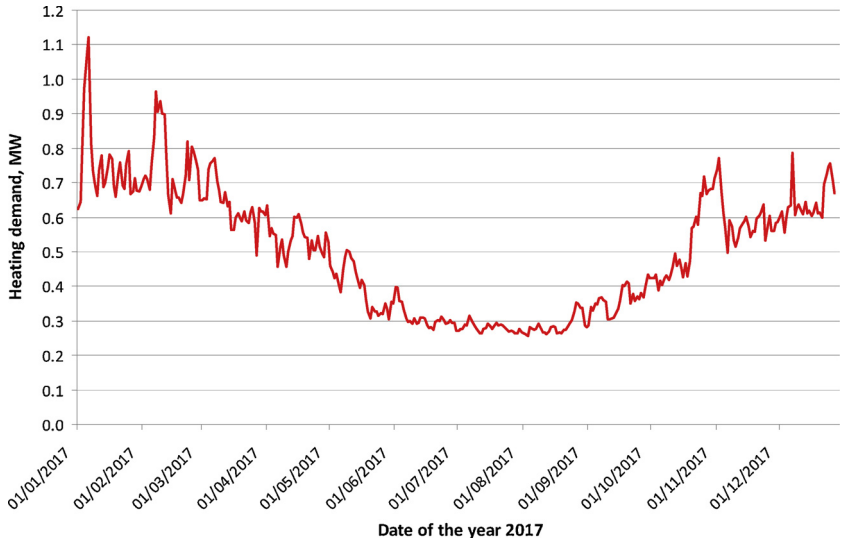

Fig. 2. Pukkila's annual heating demand.

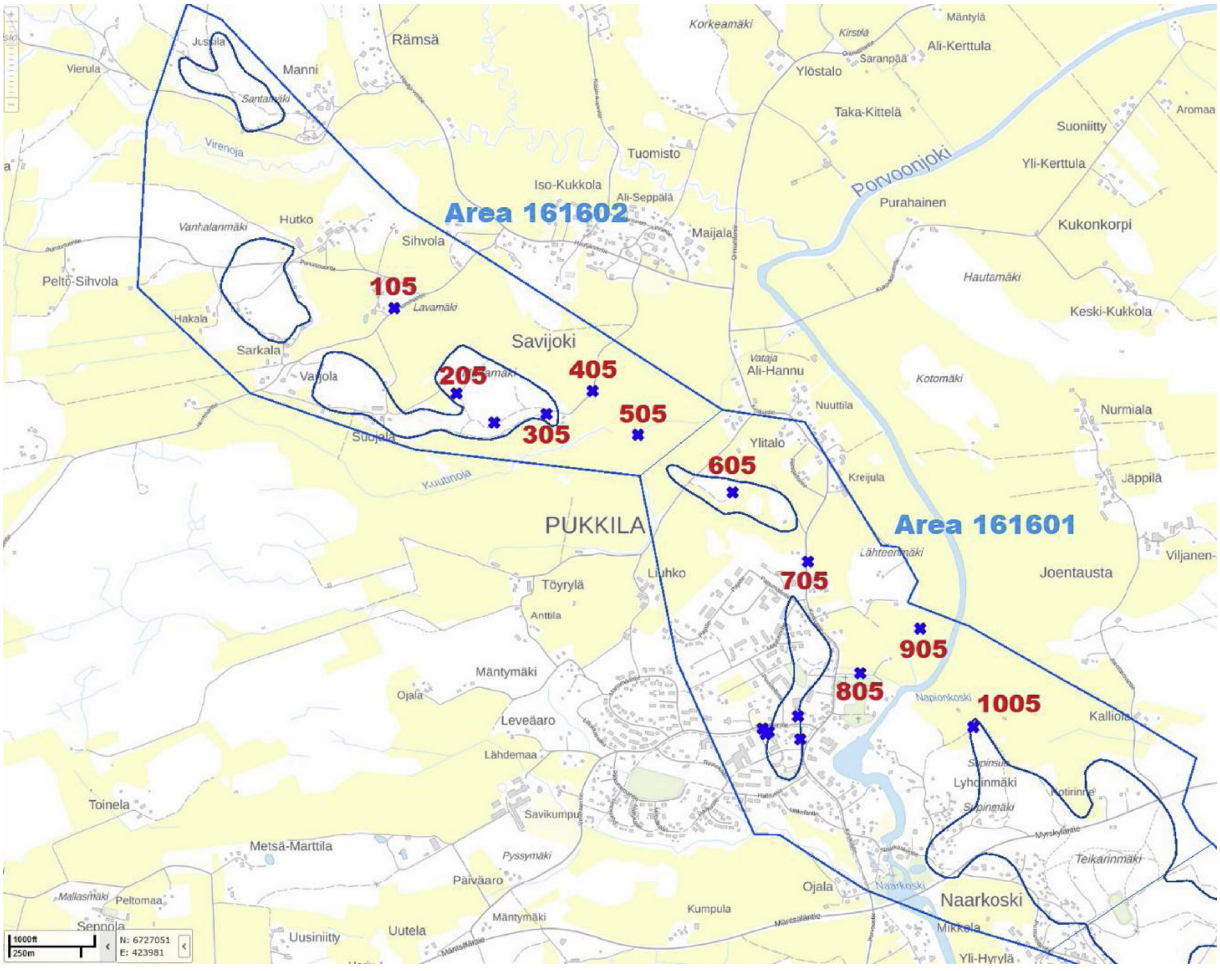

Fig. 3. Pukkila's groundwater areas.
Area #161,602 (left) and #161,601 (right), blue crosses with red numbers are the observation wells. Natural boundaries: streams Virenoja (north) and Kuutinoja (middle); Porvoonjoki River (east).

2.2. ATES integration for DH and DC

Groundwater source heat pump (GWHP), operating with warm and cold well (well doublet) is considered. For this purpose, both #605 (as warm) and #705 (as cold) wells are adopted, since they are located close to the actual district heat production plant (see Fig. 5). According to the steady state head distribution and gradient (supported by measurements of observation wells and simulations), the dominant groundwater flow is from the north (higher head values) to the south-east reaching the Porvoonjoki River as lowest head boundary.

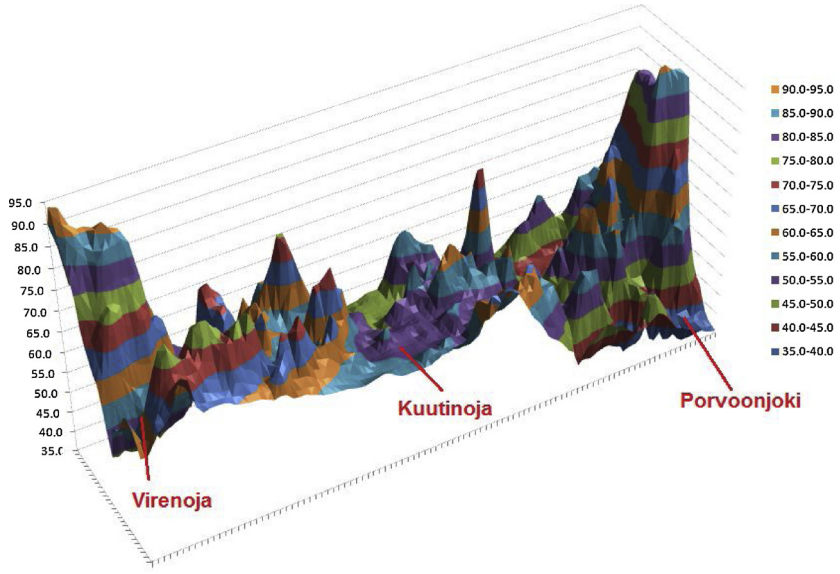

Fig. 4. Pukkila's area elevation model (3D representation).
Pukkila's area seen from west (elevation in meters above sea level, vertical scale exaggerated).

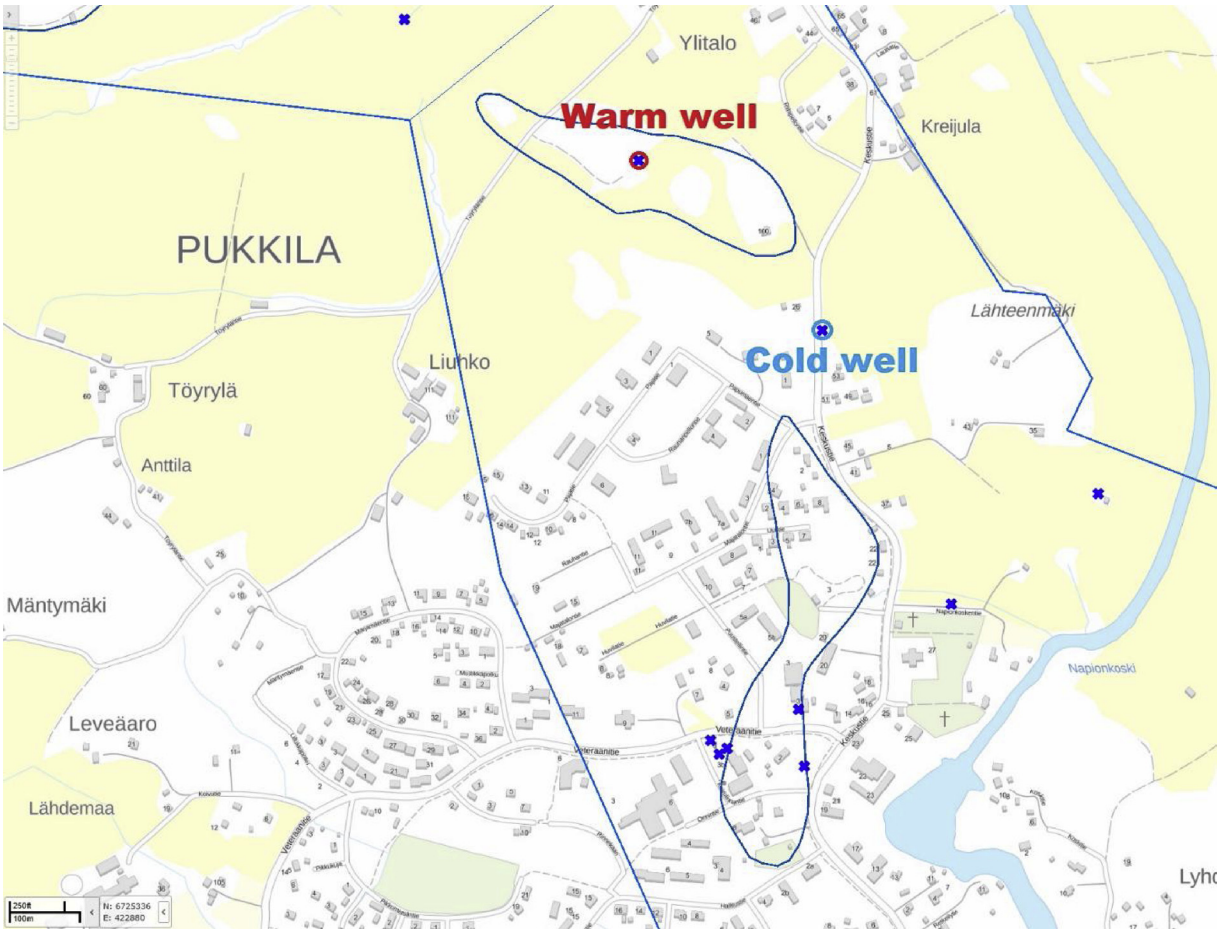

Fig. 5. Selected locations of warm and cold wells.

Hourly-based simulation results for annual heating and cooling demand of office building are used in order to introduce a dynamic variable cooling load (Tuominen, Holopainen, Eskola, Jokisalo, & Airaksinen, 2014). The data used is for a typical office building of 2695 m^2 net area and type D1 (according to Finnish building code, part C3-2010). The data was converted into an average daily-based heating and cooling loads and up-scaled appropriately (by a factor of 27) in order to match the existing Pukkila's DH network profile. GWHP is used to satisfy partially the heating demand (0.35 MW base load), using the existing chips boiler for peak loads. If boiler is needed, GWHP would be used first to increase DH network temperature from 40 °C (assumed return temperature) to some intermediate value, and after that, the final

DH supply temperature would be reached by the boiler. This would improve HP efficiency in partial load mode, since COP_H is better with lower HP supply temperature.

Different and reversible operation during summer and winter periods is assumed, creating an ATES well doublet - warm well (#605) and cold well (#705). During the summer operation a primary ATES circuit starts from the cold abstraction well, providing district cooling. After the cooling exchanger, water at up to 14 °C is utilized in GWHP evaporator, and finally injected into the warm well. During the winter period the process is reversed; water is taken from the warm well, conducted if needed through the district cooling network exchanger, used with GWHP, and finally injected into the cold well. ATES operation is simulated, calculating all relevant parameters on a daily-basis. The average pumping flow rate for each day is calculated as a maximum value between the flow needed for heating and the flow needed for cooling, using Eqs. (A.3) and (A.5). The injection temperature (after GWHP) is calculated according to Eq. (A.3) and solving for temperature drop ΔT. Finally, the electric energy demand for pumping is estimated from Eq. (A.4), assuming pumping pressure $p = 600kPa$ and overall efficiency η estimated between 0.5 and 0.6 depending on pump's size, based on producers' data for submersible pumps Grundfos SP (Grundfos, 2019). ATES reversible operation during summer and winter period is presented in Fig. 6. It should be noted that main streams are not mixed within the central flow commutation during the winter operation.

2.3. Modeling tools and methods

2.3.1. COP_H estimation model

In order to evaluate how both source temperature and heat pump

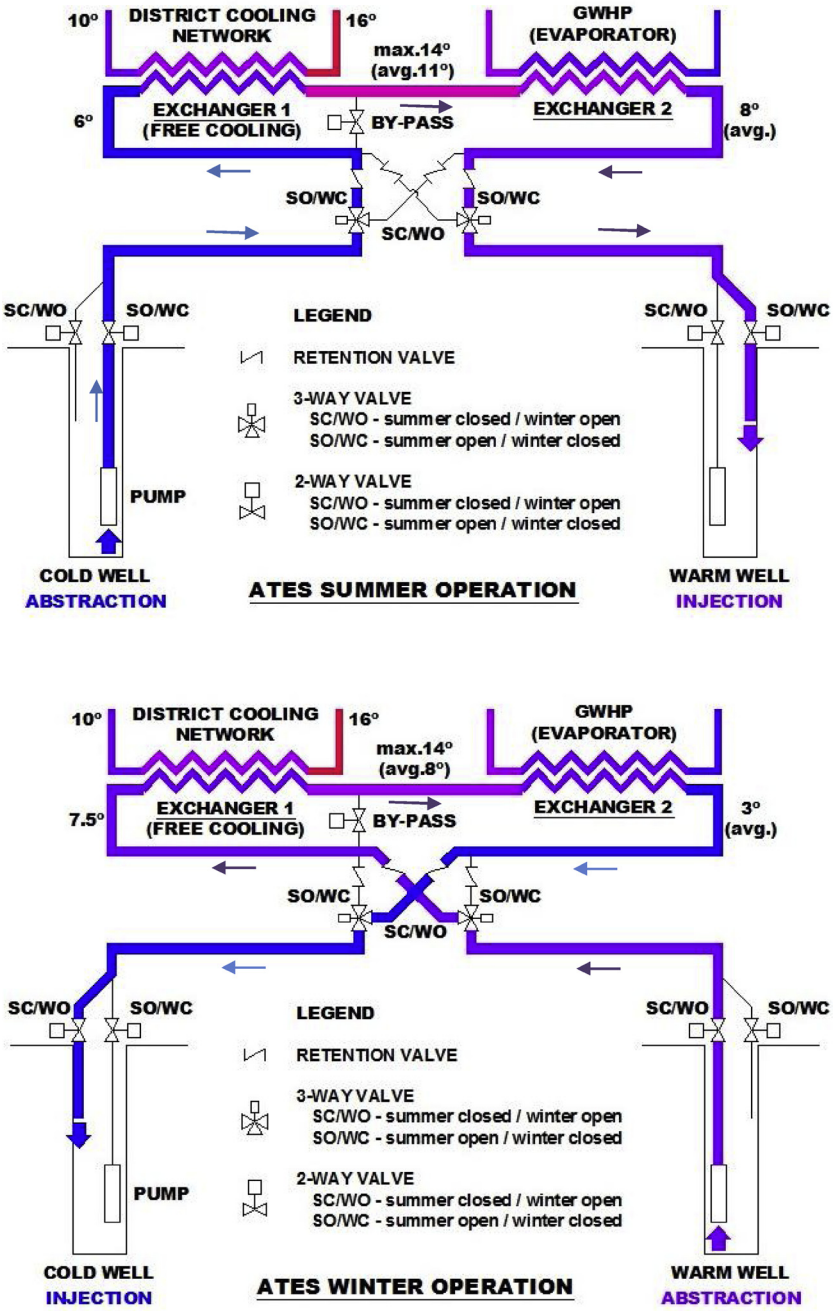

Fig. 6. Reversible ATES operation.
With different configurations of 2/3-way controlled valves, it is possible to reverse ATES operation for summer period (upper figure) and winter period (lower figure).

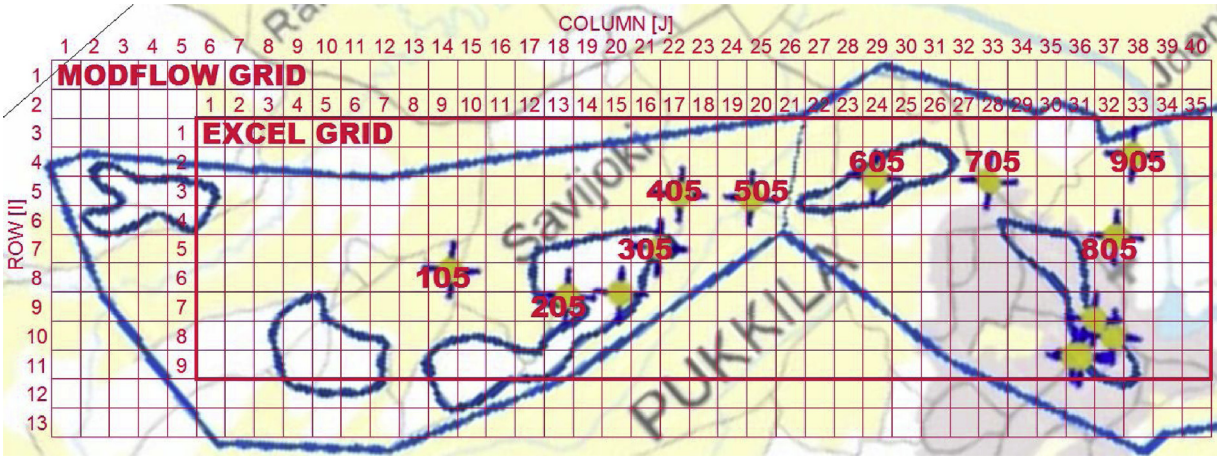

Fig. 7. Numerical models - discretization grids.
MODFLOW model contains 40 columns by 13 rows, while a simplified Excel model is a smaller sub-domain of 35 columns by 9 rows. Yellow points designate the observation wells.

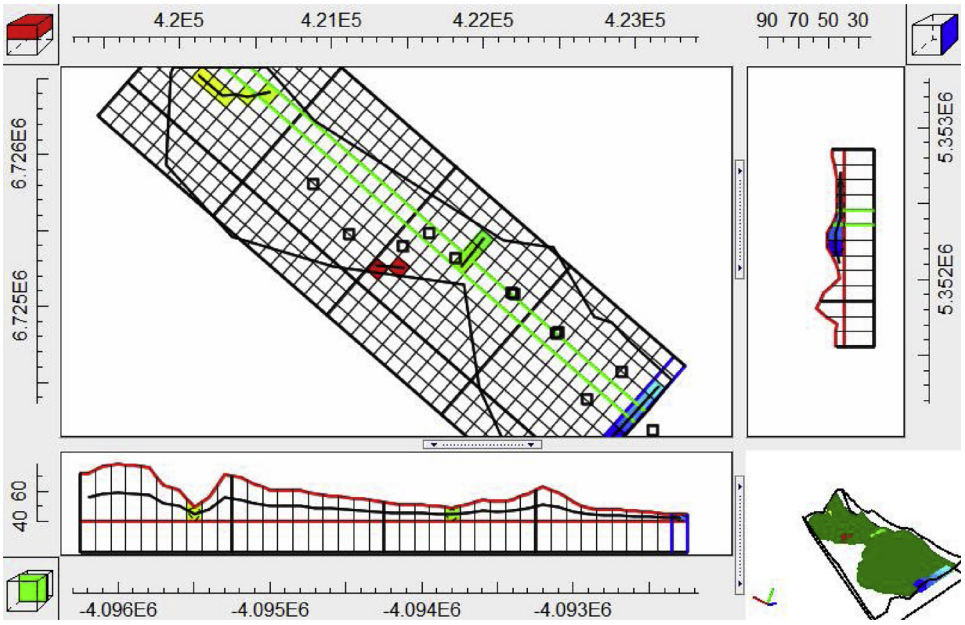

Fig. 8. Numerical models - MODFLOW environment.
Discretization grid implementation in ModelMuse (MODFLOW).

(HP) supply temperature affect GWHP efficiency, a linear regression model based on GWHP producer's data presented in the work of Pero (2016) and Hynynen (2018b), is implemented. Available data is used for four source temperatures T_1 (0°, 10°, 20° and 30°) and for five HP supply temperatures T_2 (40°, 50°, 60°, 70° and 80°). In addition, data was linearly fitted in order to obtain analytical equations for each match line (see linear regression model A.10). This linear regression model is used in all simulations, interpolating for any value of source temperatures T_1 in order to estimate heat pump COP_H as a function of T_1 and T_2.

2.3.2. Groundwater flow model

Groundwater model is a simplified quantitative tool developed in order to synthesize and represent the actual hydrological processes, as well as to be able to describe and predict their future development and trends. In order to study both the steady state and transient behavior (due to additional stresses produced e.g. from pumping), the groundwater model was developed using the finite difference code MODFLOW-2005 (Harbaugh, 2005) under ModelMuse (ModelMuse, 2019) as graphical user interface. Alternatively, a simple steady state model was created with Microsoft Excel spreadsheet in order to validate the simulated results.

2.3.3. Boundary conditions

As mentioned previously, the studied aquifer area has natural boundaries with "specified head boundary" (Dirichlet condition). Porvoonjoki River limits the area from south-east, Virenoja stream from north and Kuutinoja stream crosses the area in the middle. Aquifer north-east and south-west limits would be considered as "no flow" boundaries, special cases of "specified flow boundary" (Neumann condition) applied with zero flow. Abstraction and injection wells would be represented as point sources and modeled with "specified flow boundary". Similarly, the recharge rate is represented by a "specified flow boundary" distributed evenly over the total model area.

2.3.4. Numerical models and steady state calibration

In MODFLOW, the aquifer area is discretized using 100 × 100 m square cell and grid of 40 columns by 13 rows, covering a physical area

	48.80	48.70	48.60	48.50	48.40	48.30	48.20	48.10	48.00	
48.95	48.95	48.90	48.83	48.76	48.68	48.60	48.52	48.45	48.40	48.40
49.13	49.13	49.10	49.05	48.99	48.93	48.87	48.81	48.76	48.73	48.73
49.32	49.32	49.30	49.26	49.21	49.16	49.11	49.07	49.03	49.01	49.00
49.50	49.50	49.49	49.46	49.42	49.38	49.33	49.29	49.26	49.24	49.24
49.69	49.69	49.67	49.65	49.61	49.57	49.53	49.49	49.47	49.45	49.45
49.87	49.87	49.85	49.83	49.79	49.75	49.71	49.67	49.64	49.62	49.62
50.04	50.04	50.03	50.00	49.96	49.91	49.86	49.82	49.79	49.77	49.76
50.22	50.22	50.20	50.16	50.11	50.05	50.00	49.94	49.90	49.88	49.87
50.39	50.39	50.37	50.32	50.26	50.18	50.11	50.04	49.99	49.96	49.95
50.57	50.57	50.55	50.49	50.40	50.30	50.19	50.10	50.03	49.99	49.99
50.76	50.76	50.73	50.66	50.54	50.40	50.25	50.12	50.03	49.98	49.97
50.96	50.96	50.95	50.87	50.70	50.47	50.26	50.09	49.96	49.90	49.89
51.16	51.16	51.19	51.16	50.87	50.53	50.22	49.98	49.82	49.74	49.74
51.32	51.32	51.48	51.69	51.09	50.52	50.09	49.78	49.58	49.49	49.48
51.29	51.29	51.69	53.00	51.24	50.36	49.82	49.45	49.22	49.12	49.11
50.83	50.83	50.97	51.14	50.49	49.85	49.34	48.96	48.73	48.62	48.62
50.20	50.20	50.20	50.09	49.69	49.19	48.70	48.31	48.07	48.00	48.00
49.57	49.57	49.50	49.32	48.97	48.49	47.93	47.50	47.22	47.29	47.29
48.97	48.97	48.89	48.70	48.37	47.85	47.00	46.50	46.00	46.63	46.63
48.43	48.43	48.35	48.19	47.92	47.54	47.07	46.71	46.48	46.57	46.57
47.95	47.95	47.89	47.75	47.55	47.29	47.00	46.76	46.61	46.58	46.58
47.52	47.52	47.47	47.37	47.22	47.04	46.85	46.69	46.59	46.55	46.55
47.11	47.11	47.07	47.00	46.90	46.78	46.66	46.55	46.48	46.44	46.44
46.71	46.71	46.68	46.64	46.57	46.50	46.42	46.35	46.31	46.28	46.28
46.31	46.31	46.29	46.27	46.23	46.19	46.15	46.11	46.09	46.07	46.07
45.90	45.90	45.89	45.89	45.87	45.86	45.85	45.84	45.83	45.82	45.82
45.46	45.46	45.47	45.48	45.49	45.51	45.52	45.53	45.54	45.54	45.54
45.00	45.00	45.02	45.05	45.09	45.13	45.17	45.21	45.23	45.24	45.24
44.50	44.50	44.53	44.58	44.66	44.73	44.81	44.87	44.91	44.93	44.93
43.94	43.94	43.99	44.08	44.19	44.31	44.43	44.52	44.59	44.62	44.62
43.30	43.30	43.38	43.52	43.69	43.87	44.04	44.18	44.27	44.31	44.31
42.56	42.56	42.70	42.91	43.16	43.42	43.67	43.86	43.97	44.02	44.02
41.66	41.66	41.91	42.23	42.60	42.97	43.32	43.60	43.71	43.75	43.75
	40.50	41.00	41.50	42.00	42.50	43.00	43.50	43.50	43.50	

Fig. 9. Simplified Excel spreadsheet model in solved steady state.

of roughly 3 km^2, comprised between the aquifer north-west border and the natural boundary, Porvoonjoki River, from the east (Fig. 7).

The MODFLOW model is divided in 2 layers. Terrain's topography is introduced as "point average interpolation" for "Model_Top" parameter of the upper layer. The lower layer is a confined aquifer between elevations 20 and 40 m (see Fig. 8). A standard value for horizontal hydraulic conductivity is chosen (sand/gravel aquifer) $K_x = 1.10^{-4}$ m/s (Arola, Okkonen, & Jokisalo, 2016). Vertical hydraulic conductivity is set as $K_z = 0.1K_x$. Standard values are also used for porosity ($n = 0.25$) and storativity ($S = 1.10^{-5}$). Initially, a typical value for recharge rate of $R = 5.10^{-9}$ m/s is used (Arola et al., 2016), and after model's calibration, adjusted to $R = 6.10^{-9}$ m/s. Specified head boundaries are designated for Porvoonjoki River between 43.5 m (north) and 40.5 m (south), Virenoja stream between 48 m (east) and 48.8 m (west) and Kuutinoja from 46 – 47 m (east part) to 53 m (west part).

A simplified steady state model is implemented and calibrated using Microsoft Excel spreadsheet. For confined isotropic aquifer with recharge R and transmissivity T a two dimensional steady state groundwater model for head value h of cell (i,j) can be discretized according to Eq. (A.7). It is clear that steady state solution depends on R/T ratio, therefore in order to calibrate the model according to observation wells measured values, R/T ratio would be an important sensitive parameter to vary.

In Fig. 9, there is presented a steady state solution of a 35 × 9 cell Excel model, with heads in meters above sea level. Red border cells are specified head cells, whereas yellow cells represent a "no flow" boundary (outside model´s domain). All intermediate cells are set according to Eq. (A.7). Black border cells are the location of the observation wells (from left to right #105, 205 … 905).

Groundwater models need to be calibrated against the measured head values of the observation wells. For steady state model calibration would be used the estimated average heads between 2006 and 2016 (Anderson, Woessner, & Hunt, 2015). Trial-and-error matching was applied varying the sensitive parameter R/T between 2.10^{-6} and $3.5.10^{-6}$ using both Excel and MODFLOW groundwater models. Near-field target heads values (observation wells 605, 705, 805 and 905 in area 161,601) would have higher matching ranking than far-field heads values (Anderson et al., 2015). Root mean squared error (Eq. (A.9)) would be used as more robust indicator than a simple average and has been computed for all residual well head values, but also separately for near-field (#161,601) and far-field (#161,602) areas. The results for the best near-field match ($R = 6.10^{-9}$m/s / $T = 2.10^{-3}$ m^2/s, values finally adopted in the model) are summarized in Table 1.

2.3.5. Solute and heat transport modeling

The solute transport model MT3DMS (Bedekar et al., 2016) is used to simulate the heat transport in shallow confined aquifers due to similarities between the mathematical formulation of solute and heat transport equations (Hecht-Méndez, Molina-Giraldo, Blum, & Bayer, 2010; Hecht-Méndez, Molina-Giraldo, Blum, & Bayer, 2010). The main parameters and correlation coefficients used in MT3DMS simulation are summarized in Table 2.

2.3.6. Model implementation in MODFLOW/MT3DMS

Both winter and summer periods are simulated in MODFLOW, introducing weekly-based stress periods (injection/abstraction flows and injection temperatures of warm/cold wells are weekly averaged) as well as making local grid refinement (LGR) near the wells to improve model accuracy. Initially, abstraction temperatures from warm and cold wells are assumed as 7.5 °C and 6 °C respectively, but since these values are arbitrarily chosen, a different and novel approach is developed for estimating iteratively a convergent solution. LGR is adopted in the MODFLOW/MT3DMS model, where nearby areas to warm and cold wells are discretized with 50 × 50 m cell size (Fig. 10).

In Fig. 10, the green rectangle represents a 50 × 50 m LGR near the wells, red and blue squares represent warm and cold wells areas affected by a calculated thermal radius of roughly 75 m (Eq. (A.1)). They also are used to estimate the average abstraction temperature (during the abstraction periods). Observation point (pink) is located some 280 m downstream the cold well.

Table 1
Steady state model calibration with the ratio of R/T is 3.10^{-6}.

Observation well # [1]	Measured average head, m (2006-16) [2]	Simulated head, m Excel [3]	Residual [4]=[2]-[3] m	Simulated head, m Modflow [5]	Residual [6]=[2]-[5] m
105	50.10	50.56	-0.46	50.24	-0.14
205	53.10	51.21	1.89	50.77	2.33
305	48.70	50.57	-1.87	50.35	-1.65
405	47.60	49.17	-1.57	49.07	-1.47
505	46.60	47.58	-0.98	47.83	-1.23
605	45.90	46.72	-0.82	46.06	-0.16
705	45.10	45.72	-0.62	45.18	-0.08
805	44.30	43.99	0.31	43.77	0.53
905	43.90	44.05	-0.15	43.73	0.17
Root mean squared error (RMSE) of far-field area 161602:			1.46	-	1.54
Root mean squared error (RMSE) of near-field area 161601:			0.54	-	0.29
Root mean squared error (RMSE) both areas:			1.15	-	1.16

In the last column are highlighted the best RMSE values for MODFLOW far-field, near-field and overall results respectively.

Table 2
MT3DMS parameters and correlation coefficients.

Parameter	Symbol	Units	Value
Solid material density	ρ_s	kg/m^3	2670
Dry bulk density	ρ_b	kg/m^3	2000
Water density	ρ_w	kg/m^3	1000
Water heat capacity	c_w	J/(kg K)	4190
Solid material heat capacity	c_s	J/(kg K)	860
Porous thermal conductivity	λ_m	W/(m K)	2
Aquifer porosity	n	%	25
Distribution coefficient	K_d	m^3/kg	2.1 .10^{-4}
Diffusion coefficient	D_m	m^2/s	1.9 .10^{-6}
Longitudinal dispersivity	α	m	0.5

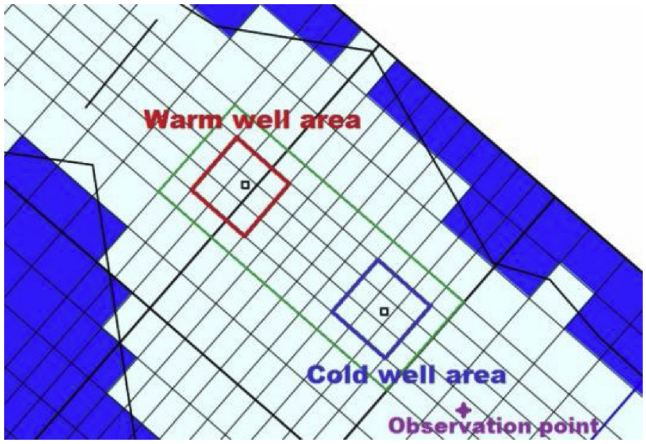

Fig. 10. Local grid refinement in nearby well areas.

2.4. Techno-economic analysis of ATES operation

In principle, it would be beneficial to limit DH network supply temperature to a maximum value of 80 °C (2018b) and reduce it according to the annual heating demand in order to limit the network losses and improve the overall efficiency. The minimum temperature of domestic hot water is recommended to be in the range 55 − 60 °C (in order to prevent the risk for *Legionella* formation, according to Banks, 2012), and therefore, the minimum recommended DH supply temperature could be established in 70 °C (Finnish Energy, 2013).

Daily-based Excel spreadsheet calculations were performed and based on them, it is possible to calculate the annual energy demands for heating, cooling and electricity as well as the average daily pumping flow rate. All relevant technical parameters are summarized in Table 3.

Cost database for different HP generation technologies is used, according to Nielsen and Möller (2013), as well as prices for piping, heat exchangers and ATES well drilling (Drenkelfort, Kieseler, Pasemann, & Behrendt, 2015) in order to determine the investment cost. The cost of produced energy is calculated based on the annuity method, assigning annual payments for the investment and taking into account the investment's lifetime of 20 years (Nielsen & Möller, 2013) as well as adopting a value of 5 % for interest rate. The annuity also includes O&M cost (assumed as 1 % of investment) and electricity cost for GWHP and ATES pumping (assumed as 100€/MWh, including taxes, transfer/distribution fees, Nordpool, 2019). The economic analysis includes the estimation of the following parameters summarized in Table 4.

3. Results and discussion

3.1. Initial ATES model settings

The annual variation of all relevant parameters is presented in Fig. 11. The annual combined demand are presented on the left axis respectively as red curve (heating) and cyan curve (cooling). Heat pump COP varies from 2.6 to 4.2 (3.4 on the average). The average injection temperature is 2.8 °C/7.9 °C (cold/warm well) and the average pumping flow rate is 0.015 m^3/s.

Summer period lasts from week 18 to week 36 (both inclusive), abstracting from cold well (#705) and injecting into the warm well (#607) respectively. Inversely, winter period comprises weeks 37–52 and 1–17, and the system operates abstracting from warm well and injecting into cold well respectively.

3.2. ATES model iterations

Additionally, an 8-year period simulation was performed with the previously developed MODFLOW model in order to study the abstraction temperature variation of the warm and the cold well, as well as to estimate the charged and discharged thermal energy. Warm/cold abstraction temperatures are calculated as an average of warm/cold well area (defined according to Fig. 10), only during the well's abstraction period (summer for the cold well and winter for the warm well). Since heating demand is dominant, charge and discharge annual cycle calculations are performed for the cold well and results are summarized in Table 5. It can be noted that after roughly 3–4 years of operation, the abstraction temperatures and heat recovery factor (HRF) converge.

Table 3
Technical parameters of ATES.

Parameter	Units	Comments
DH network flow temperature	ºC	Assumed 80 °C for days 1–60, 70 °C for days 140–260 and linearly interpolated between 70 °C and 80 °C for the rest of the year
Heat pump supply temperature T_2	ºC	Assumed as a fraction point between DH return temperature of 40 °C and DH flow temperature, depending on the fraction between GWHP heating load covered and demanded
Pumping flow rate Q	m^3/s	Calculated as maximum flow rate needed either for cooling or heating operation, since no information is available a limit of roughly 700 m^3/day per well would be considered
Heat pump COP (heating)	–	Depending on GWHP water source temperature T_1 and HP supply temperature T_2
GWHP electric power consumption	MW	Based on HP heat supply and COP
Electric power consumption for pumping	MW	Based on the calculated flow rate Q, assumed pressure head and efficiency, according to Eq. (A.4)
Aquifer injection temperature	ºC	Aquifer injection temperature T_3, Eq. (A.3)
Daily pumping flow rate	m^3/day	Average daily pumping flow rate
Annual heating demand	MWh	Heating demand supplied with GWHP
Annual cooling demand	MWh	Cooling demand supplied by ATES system
Annual electricity demand	MWh	Electricity demand of GWHP
Annual electricity demand	MWh	Electricity demand for ATES pumping

Table 4
Parameters for economic analysis.

Parameter	Units	Comments
Total investment cost	€	Based on the cost of the geological survey, GWHP and exchangers as well as well drilling and piping
Annuity factor	–	Based on Eq. (A.6), calculated for 5% interest rate and lifetime 20 years
Annual investment cost	€	Calculated as annuity factor times total investment cost
Annual fixed O&M cost	€	Estimated as 1 % of total investment cost
Annual energy cost (electricity)	€	Electricity cost for HP and pumping, based on electricity price of 100€/MWh
Total annual cost	€	Annual investment + O&M + energy costs
Cost per MWh of produced energy	€/MWh	Total annual cost divided by total energy production

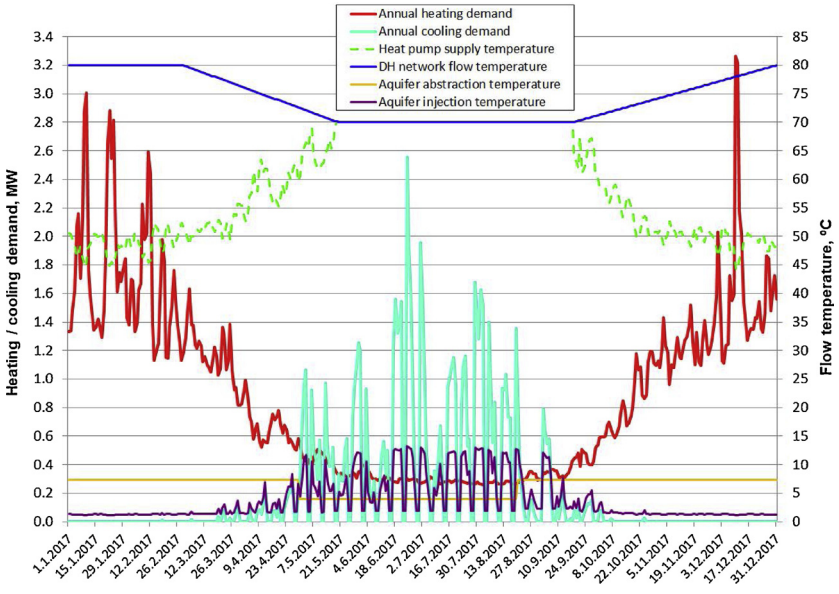

Fig. 11. ATES for combined heating and cooling (base load GWHP 0.35 MW).

Table 5
First iteration of ATES model (8-year period).

Year of operation	1	2	3	4	5	6	7	8
Annually charged energy, MWh	1230	1346	1359	1363	1364	1365	1365	1365
Annual discharged energy, MWh	844	1095	1121	1127	1129	1129	1129	1128
Heat recovery factor (HRF), cold well	0.69	0.81	0.82	0.83	0.83	0.83	0.83	0.83
Average abstraction cold well temperature, ºC	5.4	4.3	4.1	4.1	4.1	4.1	4.1	4.1
Average abstraction warm well temperature ºC	7.5	7.8	7.9	7.9	7.9	7.9	7.9	7.9

Table 6
The performance of ATES after 8 years of operation.

Model iteration	1	2	3	4
Initial warm/cold abstraction temperatures, ºC	7.5/6	7.9/4.1	7.3/4.2	7.3/3.9
Annual charged energy, MWh	1365	1295	1432	1416
Annual discharged energy, MWh	1128	990	1065	1035
Heat recovery factor (HRF)	0.83	0.76	0.74	0.73
Average abstraction cold well temperature, ºC	4.1	4.2	3.9	4.2
Average abstraction warm well temperature, ºC	7.9	7.3	7.3	7.2

From the weekly-based calculations it has also been observed that ATES summer operation should be reversed already in week 34 instead of 37. This is implemented in the next model iterations. Finally, after four iterations, warm/cold abstraction temperatures converge with good accuracy to 7.2–7.3 °C/3.9–4.2 °C, as shown in Table 6.

3.3. Techno-economic analysis

The fourth ATES model iteration is used for the analysis (warm/cold abstraction temperatures 7.3/3.9 °C). The main technical parameters of the system are summarized in Table 7. It should be noticed that even with 11 % of peak heat power, the GWHP coverage ratio is roughly 38 % of the annual heating demand. The average COP is 3.4 slightly increased to 3.6 during the winter period due to the lower GWHP supply temperature. Since heating is mostly generated during the winter period roughly 2/3 of GWHP power consumption is in winter. As the amount of pumped water is roughly balanced between winter and summer operation, the calculated thermal radius of the warm/cold wells are approximately equal (75 m). On the other hand, the excessive maximum calculated drawdown of the cold well (over 14 m) due to more intensive pumping (in only 16 weeks) during the summer period should be noted.

The economic feasibility estimation for investment costs as well as the energy production cost are presented in Tables 8 and 9 respectively. Investment costs do not include the necessary DC network implementation. The resulted overall energy production cost is roughly 41.5 €/MWh. The total investment cost is roughly 1.06 million € from which 22 % correspond to HP/exchangers and 75 % is related to the underground part (wells, pipes). These figures are in line with the research of Schüppler, Fleuchaus, and Blum (2019), where similar ATES system in Germany resulted in total investment cost of roughly 1.28 million € from which 23 % correspond to HP/exchangers and 60 % is related to wells/piping.

3.4. Impact on groundwater areas

ATES model iteration #4 is adopted in order to study the long-term effect (20 years) of warm and cold wells´ thermal interaction. The thermal front simulation of ATES operation for year 1, 2, 4, 8 and 20 is presented in the following Fig. 12, for the week when the cold and warm plumes achieve their maximum expansion.

In Fig. 12, both wells are represented by a 50 × 50 m pink cell. Left images depict the maximum annual cold well plume expansion (end of the winter period, after week 11), while right images are the maximum annual warm well plume expansion (end of the summer period, after week 31).

It can be observed that the thermal plume of the warm well maintains more or less within its thermal radius of roughly 75 m, since heat injected in the aquifer is less compared to the heat abstracted from it. Moreover, the heat plume around the warm well almost vanishes at the end of the winter period (left images), while the plume around the cold well increases slowly over the years. After 20 years of ATES operation, the thermal plume of the cold well expands several hundreds of meters to the south-east, following the dominant groundwater flow direction. All in all, it can be concluded that the locations of the wells (cold well located downstream) and the separation between them is favorable for a correct long-term ATES operation.

The temperature evolution of the warm and cold well areas over the 20-year period of ATES operation (including the observation point temperature), as well as the pumping flow rate are presented in Fig. 13. It can be acknowledged that after the third year the ATES system converges with cyclically varying temperatures: warm well 279 − 281 K, cold well 276 − 279 K. Weekly averaged pumping rates are varying between roughly 0.01 m^3/s (winter period) and $-0.025\ m^3/s$ (summer period) with some peaks when heating or cooling loads are exceptionally high. Cold plume reaches the downstream observation point after roughly 8 years of operation and after 20 years its effect is slowly attenuated to roughly −0.8 °C compared to aquifer's undisturbed temperature.

Table 7
ATES system technical parameters.

Relevant technical parameters	Annual	Winter	Summer
ATES period duration, weeks	52	36	16
GWHP peak heat power, MW	0.350	–	–
Average daily pumping flow rate, m^3/day	1,283	907	2,134
Min. / Max. daily pumping flow rate, m^3/day	711 / 5,210	711 / 2,825	1,565 / 5,210
Average abstraction temperature, ºC	6.3	7.3	3.9
Average injection temperature, ºC	3.7	2.2	7.2
Min. / Max. injection temperature, ºC	1.1 / 13.2	1.1 / 12.7	1.7 / 13.2
Average temperature entering GWHP, ºC	8.3	7.9	9.2
Min. / Max. temperature entering GWHP, ºC	3.9 / 14	7.3 / 14	3.9 / 14
Average GWHP supply temperature, ºC	58.9	54.3	69.1
Min. / Max. GWHP supply temperature, ºC	44.1 / 70	44.1 / 70	60.7 / 70
Average GWHP COP (heating mode)	3.4	3.6	2.8
Min. / Max. GWHP COP (heating mode)	2.5 / 4.1	2.7 / 4.1	2.5 / 3.4
Annual heating demand, MWh	7,749	6,888	861
Annual heating demand covered by GWHP, MWh	2,923	2,108	815
Annual heating demand covered by GWHP, %	38 %	31 %	95 %
Annual cooling demand covered, MWh	1,840	210	1,629
Annual electricity demand GWHP, MWh	882	592	290
Annual electricity demand - pumping, MWh	142	70	72
Amount of pumped water, m^3	468,426	229,364	239,061
Thermal radius, m (Eq. (A.1)) (* minimum distance between wells, defined as 3 times the average thermal radius)	225 *	74.2	75.8
Simulated drawdown (for grid cell 50 × 50 m), m	–	2.56	7.98
Calculated drawdown (for well radius 0.4 m), m (Eq. (A.8))	–	5.28	14.39

Table 8
ATES system economic parameters.

Investment cost	Price	Units	Total
Preliminary subsurface studies, pumping tests and geological report	30,000 €/unit	1	30,000 €
Groundwater source heat pump	500,000 €/MW	0.350	175,000 €
Heat exchangers	35,000 €/MW	1.750	61,250 €
Pumping well (incl. pump and equipment)	170,000 €/unit	4	680,000 €
Underground connection pipes PEHD	200 €/m	550	110,000 €
Total investment cost			**1,056,250 €**

Table 9
Energy production cost.

Energy production cost	
Annuity factor (interest rate 5 %, lifetime 20y, Eq. (A.6))	0.0802
Annual investment cost, €	84,756 €
Annual fixed O&M cost, €	10,563 €
Annual energy cost (electricity), €	102,373 €
Total annual cost, €	197,692 €
Cost per MWh of heating / cooling energy	**41.51 €**

4. Discussion

All analyses presented in this work were carried out using quite limited and uncertain information regarding the hydrogeology of the studied case area. The fundamental assumptions - normally simplified during the prefeasibility phase - were that the aquifer layer is uniform, confined and isotropic in the considered area. For more accurate aquifer parameters estimation, additional geological survey and tests for non-equilibrium (transient) flow conditions should be conducted as next steps for model calibration and validation.

The presented case study for ATES integration within DH/DC networks was economically feasible and had limited environmental impact even within a 20-year horizon of ATES operation. Combined heating and cooling demands, with seasonally reversible ATES operation and roughly balanced pumping volumes during summer and winter periods, had low impact on the aquifer area and seemed to be environmentally equilibrated.

The introduction of combined heating and cooling demand (in addition to the existing DH demand) using simulated data for typical Finnish office building was coupled with the ATES model. It showed promising economic results (energy production cost 41.5 €/MWh, compared to the average DH price in Finland of 76.7 €/MWh according to DH, 2017) and low long-term environmental impact on the surrounding groundwater areas, less than 1 °C after 20 years of operation in a radius of 280 m from the pumping wells, which is below the limits set by Swiss (3 °C) and French (11 °C) legislation. The average cold and warm storage temperatures, computed for a 20-year period of ATES operation, are 4.1 °C and 7.1 °C respectively, fulfilling the Danish limits of 2 − 25 °C. Thus, it can be concluded that the presented ATES integration for combined heating and cooling proves to be a feasible solution as well as environmentally equilibrated, fulfilling most European existing regulations.

Another important parameter is the imbalance ratio (IR), defined by Bozkaya et al. as a ratio of the difference between the heat injected and extracted from the ground and the maximum of these values. In the aforementioned research was highlighted the influence of thermal imbalance in the ground temperature change presenting variations between −10 °C and +10 °C for heating and cooling dominated systems respectively (Bozkaya, Li, & Zeiler, 2018). The current work is a case of heating dominated system with IR = −27 % and ground temperature change of roughly −1 °C after 20 years of ATES operation.

The research of this work could be continued and the result accuracy could be improved for example by the following steps:

- additional geological survey and slug & pumping tests in order to improve groundwater model quality
- detailed ATES project planning choosing the concrete well locations and their number, based on the pumping tests
- additional methods and tools for efficient input data gathering and automated data exchange between applications
- study of some additional energy sources integration, such as thermo-solar and industrial waste heat
- more detailed study on how ATES system is affected by energy prices
- more efficient ATES optimization and control strategies

5. Conclusions

The present work was successful in demonstrating that using limited and uncertain data (mostly obtained from public open-data sources), it is possible to holistically integrate groundwater models, energy demand and ATES system as well as to study system's performance efficiency, techno-economic feasibility and the impact of ATES operation on the surrounding groundwater areas. Groundwater flow and thermal models were developed and calibrated, using a variety of available data sources (National Land Survey of Finland, Finnish Environment Institute) and tools (MS Excel, QGIS, MODFLOW, MT3DMS). Heat pump COP estimation analytical model was also implemented and coupled with the groundwater models. The purpose was to develop a case study for ATES integration within the existing Pukkila's district heating network, as well as to assess the long-term environmental flow and thermal impact generated to aquifer groundwater areas.

All in all, ATES systems prove to be an efficient and a sustainable alternative for traditional fossil fuel boilers, due to their capacity to annually store and recover cooling & heating energy from the subsurface. Significant technical and economic improvement could be achieved when simultaneous or seasonable cooling and heating loads are dispatched, within integrated district energy networks.

Declaration of Competing Interest

None.

Acknowledgments

This work is part of GESATES project, an innovative initiative for groundwater heat pump application using aquifer thermal energy storage (ATES), funded by Business Finland and promoted by different participating companies and organizations, such as HELEN, Turku Energy, Nastola Foundation, Nivos Energy. It also included different research locations in Finland - Helsinki, Turku, Nastola and Pukkila-Mäntsälä region.

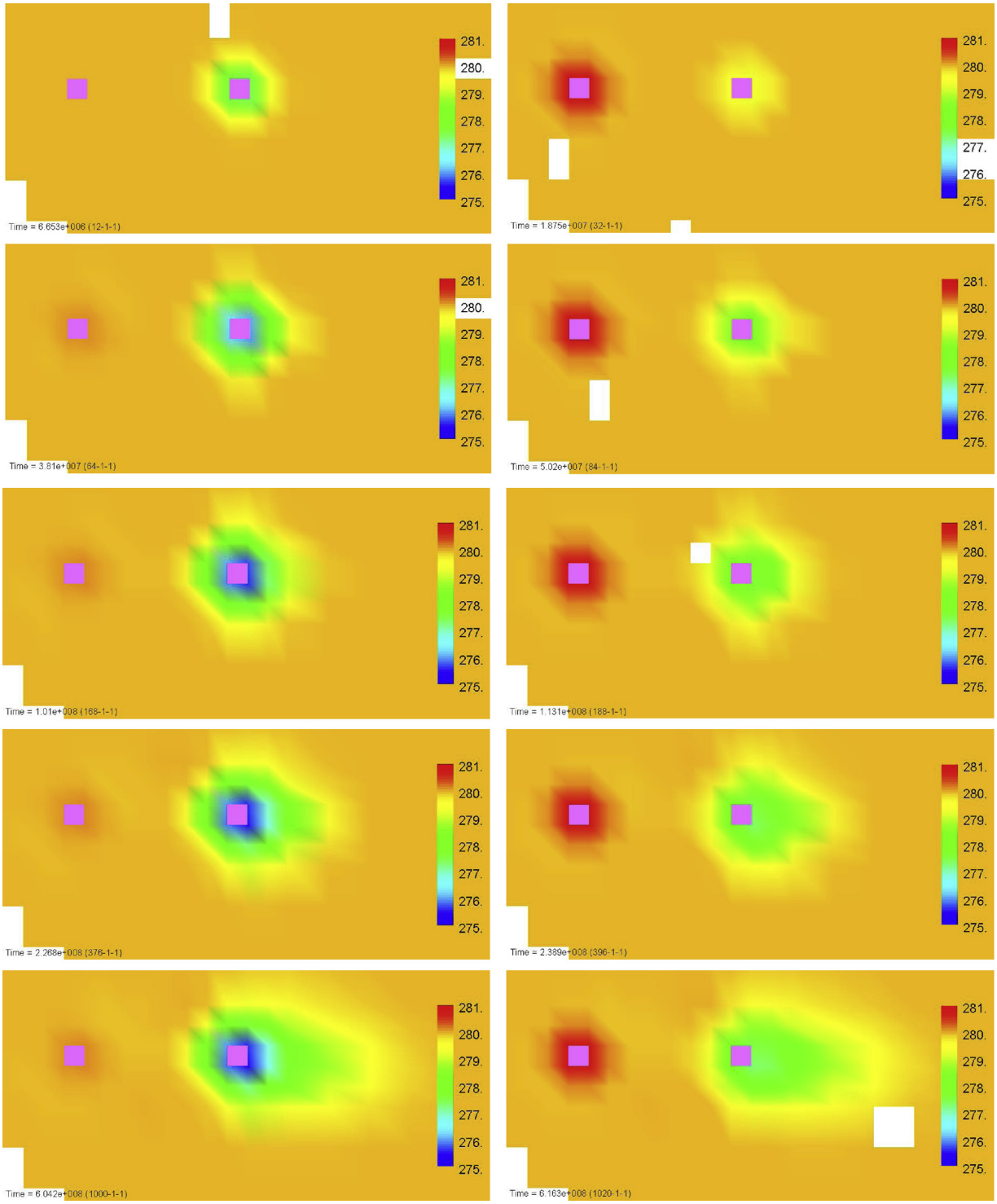

Fig. 12. Long-term thermal field evolution of ATES (years 1, 2, 4, 8 and 20).

Appendix A. Analytical solutions and formulas

- Thermal radius (Drijver & Willemsen, 2001) around the injection well r_{th} is defined as follows:

$$r_{th} = \sqrt{\frac{S_{VC,wat}\, Q}{S_{VC,aq}\, \pi b}} \tag{A.1}$$

- Heat recovery factor (*HRF*) for heating/cooling stored energy (reversible ATES operation) is defined as a ratio between the annually discharged and charged energy (Kranz and Bartels, 2010). Bloemendal et al. (2018), Bloemendal and Hartog (2018) also utilize a term of recovery efficiency, referred to a warm or cold stored energy over the whole charge/discharge cycle (normally one year):

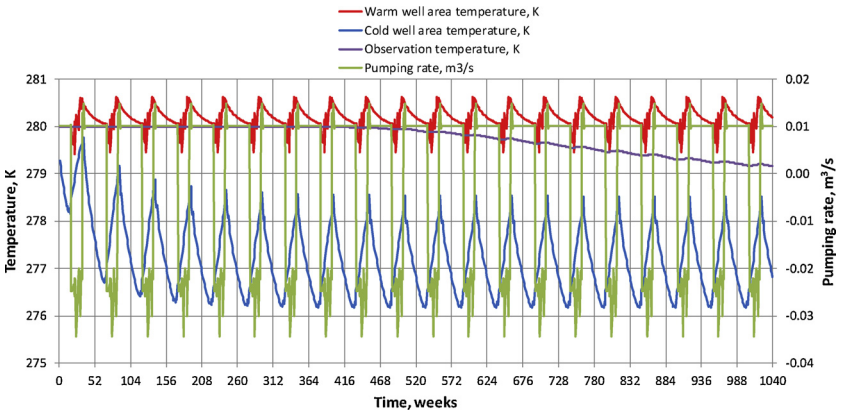

Fig. 13. 20-year period of ATES operation (thermal and flow analysis).

$$HRF = \frac{E_{out}}{E_{in}} = \frac{\int\limits_{t,out} [Q_{out}(t)\rho_w c_w (T_{warm,out}(t) - T_{cold,out}(t))]dt}{\int\limits_{t,in} [Q_{in}(t)\rho_w c_w (T_{warm,in}(t) - T_{cold,in}(t))]dt} \tag{A.2}$$

where indices *out/in* stand for discharge/charge cycles, *warm/cold* stand for warm/cold wells and E is the stored/recovered aquifer energy.

- Pumping flow rate, where Φ_i is the heat demand for a day *i* (condenser side), ΔT is water's temperature drop in heat pump evaporator side and COP_H is heat pump COP:

$$Q_i = \frac{\Phi_i\left(1 - \frac{1}{COP_H^i}\right)}{\rho_w c_w \Delta T} \tag{A.3}$$

- Electric pumping energy consumption P_i:

$$P_i = \frac{Q_i p}{\eta} \tag{A.4}$$

- Pumping flow rate, where Φ is the heat demand (evaporator side) and ΔT is water's temperature drop in heat pump evaporator side:

$$Q = \frac{\Phi}{\rho_w c_w \Delta T} \tag{A.5}$$

- Annuity factor *AF*, where r is the interest rate and k is the number of years

$$AF = \frac{r}{1 - (1 + r)^{-k}} \tag{A.6}$$

- Discretization of two dimensional steady state groundwater model for head value *h* of cell *(i,j)* for confined isotropic aquifer with recharge *R* [m/s] and transmissivity *T* [m^2/s], assuming square grid cell $\Delta x = \Delta y = a$, Fetter (2001):

$$\Rightarrow h_{i,j} = \frac{1}{4}\left(h_{i-1,j} + h_{i+1,j} + h_{i,j-1} + h_{i,j+1} + a^2\frac{R}{T}\right) \tag{A.7}$$

- Real head in cell *(i,j)* with simulated head $h_{i,j}$ containing the pumping well (with radius r_w) can be computed additionally, applying Thiem equation (according to Anderson et al., for square grid cell with side a, $r_e = 0.208a$):

$$h_w = h_{i,j} - \frac{Q}{2\pi T}\ln\frac{r_e}{r_w} \tag{A.8}$$

- Root mean squared error (*RMSE*) calculated as:

$$RMSE = \left[\frac{1}{n}\sum_{i=1}^{n}(h_m - h_s)_i^2\right]^{\frac{1}{2}} \tag{A.9}$$

where n is the number of target values, as well as h_m and h_s are respectively target measured heads and simulated head values

- Linear regression coefficients for COP_H estimation model: for $T_1 = 0\,^{\circ}C$, $a = -0.045/b = 5.5$; for $T_1 = 10\,^{\circ}C$, $a = -0.061/b = 7.06$; for $T_1 = 20\,^{\circ}C$, $a = -0.08/b = 9$; for $T_1 = 30\,^{\circ}C$, $a = -0.103/b = 11.3$

$$COP_H = a \cdot T_2 + b \tag{A.10}$$

References

Anderson, M. P., Woessner, W. W., & Hunt, R. J. (2015). *Applied groundwater modeling simulation of flow and advective transportApplied groundwater modeling* (Second Edition). https://doi.org/10.1016/B978-0-08-091638-5.00013-4.

Arola, T. (2018). *Email correspondence 17.5.2018*.

Arola, T., & Korkka-Niemi, K. (2014). The effect of urban heat islands on geothermal potential: Examples from quaternary aquifers in Finland. *Hydrogeology Journal,* 1953–1967. https://doi.org/10.1007/s10040-014-1174-5.

Arola, T., Okkonen, J., & Jokisalo, J. (2016). Groundwater utilisation for energy production in the nordic environment: An energy simulation and hydrogeological modelling approach. *Journal of Water Resource and Protection,* 642–656. https://doi.org/10.4236/jwarp.2016.86053.

Bakr, M., van Oostrom, N., & Sommer, W. (2013). Efficiency of and interference among multiple aquifer thermal energy storage systems; A Dutch case study. *Renewable Energy,* 53–62. https://doi.org/10.1016/j.renene.2013.04.004.

Banks, D. (2012). *An introduction to thermogeology: Ground source heating* (second edition). https://doi.org/10.1002/9781118447512.

Bayer, P., Attard, G., Blum, P., & Menberg, K. (2019). The geothermal potential of cities. *Renewable and Sustainable Energy Reviews, 106*, 17–30. https://doi.org/10.1016/j.rser.2019.02.019.

Bedekar, V., Morway, E., Langevin, C., & Tonkin, M. (2016). *MT3D-USGS version 1: A U.S. geological survey release of MT3DMS updated with new and expanded transport capabilities for use with MODFLOW. Techniques and methods 5-A5*369. https://doi.org/10.3133/tm6A53.

Bloemendal, M., & Hartog, N. (2018). Analysis of the impact of storage conditions on the thermal recovery efficiency of low-temperature ATES systems. *Geothermics,* 306–319. https://doi.org/10.1016/j.geothermics.2017.10.009.

Bloemendal, M., Olsthoorn, T., & Boons, F. (2014). How to achieve optimal and sustainable use of the subsurface for aquifer thermal energy storage. *Energy Policy,* 104–114. https://doi.org/10.1016/j.enpol.2013.11.034.

Bloemendal, M., Olsthoorn, T., & van de Ven, F. (2015). Combining climatic and geo-hydrological preconditions as a method to determine world potential for aquifer thermal energy storage. *Science of the Total Environment,* 621–633. https://doi.org/10.1016/j.scitotenv.2015.07.084.

Bloemendal, M., Jaxa-Rozen, M., & Olsthoorn, T. (2018). Methods for planning of ATES systems. *Applied Energy,* 534–557. https://doi.org/10.1016/j.apenergy.2018.02.068.

Bonafoni, S., Baldinelli, G., & Verducci, P. (2017). Sustainable strategies for smart cities: Analysis of the town development effect on surface urban heat island through remote sensing methodologies. *Sustainable Cities and Society, 29*, 211–218. https://doi.org/10.1016/j.scs.2016.11.005.

Bonte, M., Stuyfzand, P. J., Hulsmann, A., & van Beelen, P. (2011). Underground thermal energy storage: Environmental risks and policy developments in the Netherlands and European Union. *Ecology and Society, 16*(1), 22. https://doi.org/10.5751/ES-03762-160122.

Bozkaya, B., Li, R., Labeodan, T., Kramer, R., & Zeiler, W. (2017). Development and evaluation of a building integrated aquifer thermal storage model. *Applied Thermal Engineering,* 620–629. https://doi.org/10.1016/j.applthermaleng.2017.07.195.

Bozkaya, B., Li, R., & Zeiler, W. (2018). A dynamic building and aquifer co-simulation method for thermal imbalance investigation. *Applied Thermal Engineering, 144*, 681–694. https://doi.org/10.1016/j.applthermaleng.2018.08.095.

Caljé, R. J. (2010). *Future use of aquifer thermal energy storage below the historic center of Amsterdam*.

DH (2017). *District heating in Finland 2017, Energiateollisuus ry 2018 (Finnish Energy)*. ISSN 0786-4809 (Accessed 30 September 2019)https://energia.fi/files/2948/District_heating_in_Finland_2017.pdf.

Drenkelfort, G., Kieseler, S., Pasemann, A., & Behrendt, F. (2015). Aquifer thermal energy storages as a cooling option for German data centers. *Energy Efficiency,* 385–402. https://doi.org/10.1007/s12053-014-9295-1.

Drijver, B., & Willemsen, A. (2001). *Groundwater as a heat source for geothermal heat pumps* (Accessed 24 May 2019)https://www.geothermal-energy.org/pdf/IGAstandard/ISS/2003Germany/II/7_1.dri.pdf.

EU (2013). *Energy efficiency buildings in the EU trends—Lessons from the ODYSSEE MURE project.* ADEME.

Fetter, C. W. (2001). *Applied hydrogeology* (fourth edition). .

Finnish Energy (2013). *District heating of buildings. Regulations and guidelines* (Accessed 24 May 2019)Publication K12013https://energia.fi/files/1555/DH_of_buildings_PublicationK1_EN.pdf.

Fleuchaus, P., Godschalk, B., Stober, I., & Blum, P. (2018). Worldwide application of aquifer thermal energy storage—A review. *Renewable and Sustainable Energy Reviews,* 861–876. https://doi.org/10.1016/j.rser.2018.06.057.

Fleuchaus, P., Schüppler, S., Godschalk, B., Bakema, G., & Blum, P. (2020). Performance analysis of aquifer thermal energy storage (ATES). *Renewable Energy, 146*, 1536–1548. https://doi.org/10.1016/j.renene.2019.07.030 ISSN 0960-1481.

Ghaebi, H., Bahadori, M. N., & Saidi, M. H. (2014). Performance analysis and parametric study of thermal energy storage in an aquifer coupled with a heat pump and solar collectors, for a residential complex in Tehran, Iran. *Applied Thermal Engineering,* 156–170. https://doi.org/10.1016/j.applthermaleng.2013.09.037.

Grundfos, S.P., Submersible pumps. (Accessed 23 May 2019). https://www.grundfos.com/products/find-product/sp.html.

Haehnlein, S., Bayer, P., & Blum, P. (2010). International legal status of the use of shallow geothermal energy. *Renewable and Sustainable Energy Reviews,* 2611–2625. https://doi.org/10.1016/j.rser.2010.07.069.

Harbaugh, A. W. (2005). *MODFLOW-2005, the U.S. geological survey modular ground-water model—The ground-water flow process. U.S. Geological survey techniques and methods 6-A15*https://doi.org/10.3133/tm6A16.

Hecht-Méndez, J., Molina-Giraldo, N., Blum, P., & Bayer, P. (2010a). Evaluating MT3DMS for heat transport simulation of closed geothermal systems. *Ground Water,* 741–756. https://doi.org/10.1111/j.1745-6584.2010.00678.x.

Hecht-Méndez, J., Molina-Giraldo, N., Blum, P., & Bayer, P. (2010b). Use of MT3DMS for heat transport simulation of shallow geothermal systems. *Proceedings World Geothermal Congress*.

Hooimeijer, F., & Maring, L. (2018). The significance of the subsurface in urban renewal. *Journal of Urbanism: International Research on Placemaking and Urban Sustainability, 11*(3), 303–3328. https://doi.org/10.1080/17549175.2017.1422532.

Hoving, J., Bozkaya, B., Zeiler, W., Haan, J. F., Boxem, G., & van der Velden, J. A. J. (2014). Thermal storage capacity control of aquifer systems. *BauSim* (pp. 617–625).

Hynynen, H. (2018a). *Email correspondence (20.4.2018)*.

Hynynen, H. (2018b). *Flow temperature reduction in the development of a district heating network*. https://aaltodoc.aalto.fi/handle/123456789/32370.

Kastner, O., Norden, B., Klapperer, S., Park, S., Urpi, L., Cacace, M., et al. (2017). Thermal solar energy storage in Jurassic aquifers in Northeastern Germany: A simulation study. *Renewable Energy,* 290–306. https://doi.org/10.1016/j.renene.2016.12.003.

Kranz, S., & Bartels, J. (2010). *Simulation and Data Based Optimisation of an Operating Seasonal Aquifer Thermal Energy Storage. Proceedings World Geothermal Congress.* Indonesia: Bali.

Lu, H., Tian, P., & He, L. (2019). Evaluating the global potential of aquifer thermal energy storage and determining the potential worldwide hotspots driven by socio-economic, geo-hydrologic and climatic conditions. *Renewable and Sustainable Energy Reviews, 112*, 788–796. https://doi.org/10.1016/j.rser.2019.06.013.

Lund, J. W., & Boyd, T. L. (2016). Direct utilization of geothermal energy 2015 worldwide review. *Geothermics,* 66–93. https://doi.org/10.1016/j.geothermics.2015.11.004.

ModelMuse: A graphical user interface for groundwater models: https://www.usgs.gov/software/modelmuse-a-graphical-user-interface-groundwater-models. (Accessed 23 May 2019).

Nielsen, S., & Möller, B. (2013). GIS based analysis of future district heating potential in Denmark. *Energy,* 458–468. https://doi.org/10.1016/j.energy.2013.05.041.

Nordpool Finnish monthly prices 2005—2018. (Accessed 22 May 2019). https://www.nordpoolgroup.com/Market-data1/Dayahead/Area-Prices/FI/Monthly/?dd=FI&view=table.

Paiho, S., Saastamoinen, H., Hakkarainen, E., Similä, L., Pasonen, R., Ikäheimo, J., et al. (2018). Increasing flexibility of Finnish energy systems—A review of potential technologies and means. *Sustainable Cities and Society, 43*, 509–523. https://doi.org/10.1016/j.scs.2018.09.015.

Paksoy, H. O., Andersson, O., Abaci, S., Evliya, H., & Turgut, B. (2000). Heating and cooling of a hospital using solar energy coupled with seasonal thermal energy storage in an aquifer. *Renewable Energy,* 117–122. https://doi.org/10.1016/S0960-1481(99)00060-9.

Pellegrini, M., Bloemendal, M., Hoekstra, N., Spaak, G., Andreu Gallego, A., Rodriguez Comins, J., et al. (2019). Low carbon heating and cooling by combining various technologies with aquifer thermal energy storage. *Science of the Total Environment,* 1–10. https://doi.org/10.1016/j.scitotenv.2019.01.135.

Pero, J. (2016). *District heating business development in Mäntsälän Sähkö limited company* (Accessed 24 May 2019)http://lutpub.lut.fi/bitstream/handle/10024/123395/diplomityo_pero_juha.pdf.

QGIS - The leading open source desktop GIS. (Accessed 23 May 2019). https://www.qgis.org/en/site/about/index.html.

Sanner, B. (2001). Shallow geothermal energy. *Geo-Heat Center Bulletin*. (Accessed 24 May 2019) https://geothermalcommunities.eu/assets/elearning/6.2.art4.pdf.

Schmidt, T., Pauschinger, T., Sørensen, P. A., Snijders, A., & Thornton, J. (2018). Design aspects for large-scale pit and aquifer thermal energy storage for district heating and cooling. *Energy Procedia, 149*(September), 585–594. https://doi.org/10.1016/j.egypro.2018.08.223.

Schüppler, S., Fleuchaus, P., & Blum, P. (2019). Techno-economic and environmental analysis of an aquifer thermal energy storage (ATES) in Germany. *Geothermal Energy, 7*(1), 1–24. https://doi.org/10.1186/s40517-019-0127-6.

Sommer, W., Valstar, J., Leusbrock, I., Grotenhuis, T., & Rijnaarts, H. (2015). Optimization and spatial pattern of large-scale aquifer thermal energy storage. *Applied Energy,* 322–337. https://doi.org/10.1016/j.apenergy.2014.10.019.

Tuominen, P., Holopainen, R., Eskola, L., Jokisalo, J., & Airaksinen, M. (2014). Calculation method and tool for assessing energy consumption in the building stock. *Building and Environment,* 153–160. https://doi.org/10.1016/j.buildenv.2014.02.001.

UN (2015). *Adoption of the Paris agreement, report no. FCCC/CP/2015/L.9/Rev.1. Adoption of the Paris agreement*https://www.doi.org/FCCC/CP/2015/L.9/Rev.1.

Zheng, C., & Wang, P. P. (1999). *MT3DMS: A modular three-dimensional multispecies transport model for simulation of advection, dispersion and chemical reactions of contaminants in groundwater systems; Documentation and user's Guide. Contract Report SERDP-99-1vol. 220*. US Army Corps of Engineers, Engineer Research and Development Center.